High-spin states in ^{127}I

B. Ding (丁兵),[1,2] Y. H. Zhang (张玉虎),[1,*] X. H. Zhou (周小红),[1] G. X. Dong (董国香),[3] F. R. Xu (许甫荣),[3]
M. L. Liu (柳敏良),[1] G. S. Li (李广顺),[1,2] N. T. Zhang (张宁涛),[1] H. X. Wang (王海霞),[1,2] H. B. Zhou (周厚兵),[1,2]
Y. J. Ma (马英君),[4] Y. Sasakiz,[5] K. Yamada,[5] H. Ohshima,[5] S. Yokose,[5] M. Ishizuka,[5] T. Komatsubara,[5] and K. Furuno[5]

[1]*Institute of Modern Physics, Chinese Academy of Sciences, Lanzhou 730000, China*
[2]*Graduate School of Chinese Academy of Sciences, Beijing 100049, China*
[3]*Department of Technical Physics and MOE Key Laboratory, Peking University, Beijing 100871, China*
[4]*Department of Physics, Jilin University, Changchun 130021, China*
[5]*Institute of Physics and Tandem Accelerator Center, University of Tsukuba, Ibaraki 305-0006, Japan*

(Received 1 November 2011; revised manuscript received 29 February 2012; published 9 April 2012)

In-beam γ spectroscopy of the stable nucleus ^{127}I has been studied experimentally using the ^{124}Sn(^{7}Li, $4n\gamma$)^{127}I reaction at a beam energy of 32 MeV. The high-spin level scheme of ^{127}I is extended significantly. Negative-parity levels built on the $11/2^-$, $\pi h_{11/2}$ particle state are observed up to $(35/2^-)$ and described as a decoupled band, extending our knowledge of decoupled structures to the most neutron-rich stable iodine isotope. Two $\Delta I = 2$ yrast positive-parity sequences are proposed to be associated with the $\pi g_{7/2}$ configuration due to observations of several strong interband transitions, and two weakly populated $\Delta I = 2$ positive-parity bands are newly identified and interpreted as arising mainly from the $\pi d_{5/2}$ configuration. Three-quasiparticle configurations are assigned to the $I^\pi = 15/2^+$ and $23/2^+$ states according to the existing knowledge in neighboring nuclei; irregular noncollective and regular collective excitations built on these two ($15/2^+$ and $23/2^+$) states are observed to coexist at similar energies. The observed three-quasiparticle band structures are further interpreted with the aid of configuration-constrained potential energy surface calculations.

DOI: 10.1103/PhysRevC.85.044306 PACS number(s): 21.10.Re, 23.20.Lv, 25.70.Gh, 27.60.+j

I. INTRODUCTION

A general feature of transitional nuclei in the $A \sim 130$ mass region is the softness of the nuclear potential. For an odd-A nuclide, the valence particle occupying different Nilsson orbitals outside the doubly-even core may influence the core shape differently due to the well-known polarization effect [1,2]. Iodine nuclei, with $Z = 53$, display the characteristic features of transitional nuclei. A large number of bands with the odd proton occupying the different Nilsson orbitals near the Fermi level were observed in the iodine isotopes [3]. Among these bands, two collective features were systematically identified. One is the $\Delta I = 1$ rotational band built on the low-lying deformed $9/2^+$ proton-hole intruder state resulting from the excitation of a $1g_{9/2}$ proton across the $Z = 50$ closed shell [3,4]. The other one involves $\Delta I = 2$ bands built on the $11/2^-_1$, $7/2^+_1$, and $5/2^+_1$ states [3,5]. The level spacings of the $\Delta I = 2$ bands generally follow those of the ground state (g.s.) bands of the corresponding even-even core nuclei, and hence these bands were described as decoupled bands based on the $\pi h_{11/2}$, $\pi g_{7/2}$, and $\pi d_{5/2}$ configurations. However, with the development of measurement techniques, the interband dipole transitions between the members of the $\pi g_{7/2}$ and $\pi d_{5/2}$ "decoupled bands" were found experimentally in ^{121,123,125}I [6–8]. Thus, an alternative description was proposed for the two $\Delta I = 2$ bands; i.e., the two decoupled bands were interpreted as a $\Delta I = 1$ band based on the $\pi d_{5/2}/\pi g_{7/2}$ mixed configuration. In addition, such coupled structures can be well reproduced with oblate deformations in ^{121,123,125}I [2,9,10], supporting such an alternative interpretation.

Three-quasiparticle (three-QP) bands starting at intermediate spins ($I = 19/2,\ 21/2$, etc.) were reported in many odd-A nuclei in this mass region [8,11,12]. The configurations of these bands involve the odd proton being coupled to the two-QP states in the neighboring even-even core nuclei. The rotational level structure gives way to a more complex single-particle structure at high spins, resulting in a band termination. The terminating states at $I^\pi = 39/2^-$ and $43/2^-$ were systematically identified in odd-A iodine isotopes (see Ref. [13] and references therein). More interestingly, both collective and noncollective states were found to coexist at high spins in these nuclei [14,15].

In this paper, we report the experimental results on high-spin band structures in ^{127}I using standard in-beam γ-ray spectroscopy techniques. Prior to this work, low-spin states in ^{127}I were established from Coulomb excitation [16] and β-decay studies of ^{127}Te^m and ^{127}Te^g [17]. Later, high-spin states up to $23/2^-$ and $21/2^+$ were identified through in-beam γ spectroscopy [4]. The aim of the present investigation is to probe the above-mentioned structural features in ^{127}I in order to complete the systematics of level structures in odd-mass iodine isotopes, and to provide more information for a deeper understanding of nuclear structures in transitional nuclei in the $A \sim 130$ region.

II. EXPERIMENT AND RESULTS

A. Measurements

The experiment was performed at the tandem accelerator laboratory at the University of Tsukuba, Japan. High-spin states in ^{127}I were populated using the heavy-ion induced fusion-evaporation reaction ^{124}Sn(^{7}Li,$4n\gamma$)^{127}I at a beam

*yhzhang@impcas.ac.cn

energy of 32 MeV. The target was an enriched self-supporting ^{124}Sn metallic foil with a thickness of 4 mg/cm^2. A γ-ray detector array [18] consisting of one planar detector and nine BGO–Compton-suppressed high-purity germanium (Ge) detectors was used to measure the in-beam γ rays. Five Ge detectors were positioned at 37° and the others near 90° with respect to the beam direction. The distance between the target and the detectors was on average 13 cm. The energy and efficiency calibrations were made using ^{152}Eu and ^{133}Ba standard sources. Typical energy resolutions were about 2.0–2.5 keV at full width at half maximum (FWHM) for the 1332.5-keV line. A total of 67 million γ-γ-t (Here, t refers to the relative time difference between any two coincident γ rays detected within ±100 ns) coincidence events were accumulated. After accurate gain matching for all the detectors, these coincidence events were sorted into a symmetric matrix for subsequent off-line analysis.

In order to obtain multipolarity information for the emitting γ rays, the coincidence data were sorted into two asymmetric matrices whose x axis was the γ-ray energy deposited in the detectors at any angle and whose y axis was the γ-ray energy deposited in the detectors at 37° (or 143°) and 90°, respectively. From these two matrices, the angular distribution asymmetry ratios, defined as $R_{\mathrm{ADO}}(\gamma) = I_\gamma(37^\circ)/I_\gamma(90^\circ)$, were extracted from the γ-ray intensities $I_\gamma(37^\circ)$ and $I_\gamma(90^\circ)$ in the coincidence spectra gated by the γ transitions (on the x axis) of any multipolarity. Usually, a single gate was used for strong peaks. For some weak or doublet peaks, the gating transitions were carefully chosen in order to obtain clear coincidence spectra in which possible contaminations to the transition of interest can be excluded. In such an analysis, typical γ-ray Angular Distribution of γ rays Deexciting the Oriented States (ADO) ratios for the known γ rays observed in this experiment were 1.29 for stretched quadrupole transitions and 0.75 for stretched pure dipole transitions. Therefore, we assigned the stretched quadrupole transition and stretched dipole transition to the γ rays of ^{127}I with ADO values around 1.29 and 0.75, respectively.

B. Level scheme

Most of the γ rays reported in the previous literature belonging to ^{127}I [4] were observed in this experiment. The γ-γ coincidence relationships have been analyzed with care, leading to the establishment of the extended level scheme for ^{127}I. The ordering of transitions in the level scheme was determined according to the γ-ray relative intensities, γ-γ coincidence relationships, and γ-ray energy sums. The transition character was deduced from the measured ADO ratios. In assigning spins and parities to the levels observed, $E2$ multipolarity is assumed for stretched quadrupole transitions. $E1$ or $M1$ character is possible for the dipole transitions. The $M1$ transition may have $E2$ admixture. The spins and parities for the known low-lying states were adopted from the previous work [4], and these values were used as the references of the spin and parity assignments for the higher spin states. In the present work, we used the general yrast argument that levels populated in heavy-ion reactions usually have spins increasing with increasing excitation energy. Therefore, the measured ADO ratios allow straightforward determinations of spins and parities for the excited states in ^{127}I. The measured spectroscopic data (γ-ray energies, relative intensities, ADO ratios, and suggested spin and parity assignments) are summarized in Table I. The level scheme of ^{127}I deduced from the present work is shown in Fig. 1 and labeled A–F. Bands A and B were previously known [4] and have been extended to higher spin states, whereas level structures C, D, E, and F have been newly established in the present experiment. Some brief explanations of the level scheme are given in the following.

The cascade of $\Delta I = 2$ transitions labeled A in Fig. 1 was reported up to the $23/2^-$ state in Ref. [4]. All these transitions and their quadrupole character were confirmed in the present work. In addition, several new γ rays above the $23/2^-$ state are observed and placed in the level scheme extending the sequence up to the $35/2^-$ state at 5242.7 keV. The placement and ordering for the newly observed transitions are supported by the parallel and crossover transitions as shown in Fig. 1. The deduced ADO ratios given in Table I show stretched quadrupole character for the 981.8-, 1012.5-, 653.1-, and 601.0-keV γ rays and dipole character for the 409.5-, 378.9-, and 274.2-keV lines. These results support the spin and parity assignments for the levels above the $23/2^-$ state. The coincidence spectrum gated on the 651.5-keV γ ray is shown in Fig. 2(a), displaying the transitions associated with the negative-parity states.

The positive-parity band B built on the 57.4-keV state was populated most strongly in this experiment. The ordering of the transitions in this band was fixed firmly with the observation of interband transitions. The two $\Delta I = 2$ sequences of this band were established previously [4] up to the $19/2^+$ and $21/2^+$ states, respectively, by adding 880- and 934-keV transitions to the yrast $15/2^+$ and $17/2^+$ states. Checking carefully the γ-ray energies, we found that these two γ rays should be the 877.0- and 930.3-keV lines observed in this experiment; several parallel crossover transitions deexciting the new level at 2901.2 keV support the placements of the associated γ transitions and γ-ray energies determined in this work. The new 850.5-, 912.4-, and 812.3-keV γ rays of stretched quadrupole character are observed and placed in the level scheme extending the two $\Delta I = 2$ sequences up to the $23/2^+$ and $25/2^+$ states, respectively. In addition to the in-band transitions, several interband transitions linking the two $\Delta I = 2$ sequences are newly observed. As shown in Fig. 3, transitions associated with band B can be seen in the coincidence γ-ray spectra.

Apart from the yrast positive-parity band discussed above, two $\Delta I = 2$ cascades labeled C are newly observed, feeding the $5/2^+$ g.s. and the second $7/2^+$ state. The linking transitions with bands A and B as well as the weak interband transitions fix the ordering and the spin and parity of the associated levels in band C. Representative coincidence spectra demonstrating the existence of band C are shown in Fig. 3, in which some intense linking and interband transitions can be clearly identified. The 806-keV transition is found to be a doublet; the 806.4-keV transition is assigned to feed the 1550.7-keV level while the 805.9-keV γ ray deexcites this state. Their placements and γ-ray energies are unambiguously confirmed by the weak

TABLE I. γ-ray transition energies, relative intensities, ADOratios, and their assignments in ^{127}I.

E_γ(keV)[a]	I_γ[b]	R_{ADO}[c]	$E_i \rightarrow E_f$ (keV)[d]	$I_i^\pi \rightarrow I_f^\pi$[e]
57.4	745	0.96(10)	57.4 → 0	$7/2^+ \rightarrow 5/2^+$
80.0	82	0.82(8)	2423.2 → 2343.0	$(19/2^+) \rightarrow (17/2^+)$
94.8	63	0.82(8)	2901.2 → 2806.3	$23/2^+ \rightarrow 21/2^+$
112.8	74	0.73(7)	2901.2 → 2788.4	$23/2^+ \rightarrow 21/2^+$
116.2	10	0.80(10)	744.8 → 628.5	$9/2^+ \rightarrow 7/2^+$
144.4	11	1.06(37)	2068.4 → 1924.0	$(15/2^+) \rightarrow (13/2)$
155.7	28	0.81(8)	2806.3 → 2650.5	$21/2^+ \rightarrow (19/2^+)$
157.5	13	0.80(19)	2315.5 → 2157.9	$(15/2) \rightarrow (13/2)$
159.3	57	0.66(7)	2846.3 → 2687.0	$(21/2^+) \rightarrow (19/2^+)$
174.7	144	1.20(12)	2068.4 → 1893.7	$(15/2^+) \rightarrow 15/2^-$
187.5	⩽10		2976.2 → 2788.4	$23/2^- \rightarrow 21/2^+$
188.0	10		2545.2 → 2357.2	$19/2^- \rightarrow 17/2^+$
189.1	23	1.35(14)	2612.3 → 2423.2	$(19/2^+) \rightarrow (19/2^+)$
195.4	112	0.85(8)	2612.3 → 2417.0	$(19/2^+) \rightarrow (17/2^+)$
195.8	38	0.68(7)	2846.3 → 2650.5	$(21/2^+) \rightarrow (19/2^+)$
213.1	25	0.75(8)	2477.9 → 2264.6	$(17/2) \rightarrow (15/2)$
213.5	76	0.75(10)	1479.7 → 1266.3	$15/2^+ \rightarrow 13/2^+$
214.8	210	0.72(7)	3116.0 → 2901.2	$25/2^+ \rightarrow 23/2^+$
240.3	20	0.95(14)	2264.6 → 2024.0	$(15/2) \rightarrow (13/2)$
243.0	16	1.25(30)	3031.4 → 2788.4	$(25/2^+) \rightarrow 21/2^+$
244.0	10		1550.7 → 1306.5	$13/2^+ \rightarrow 11/2^+$
247.3	28	1.15(10)	2315.5 → 2068.4	$(15/2) \rightarrow (15/2^+)$
250.6	15	1.42(21)	2901.2 → 2650.5	$23/2^+ \rightarrow (19/2^+)$
253.6	106	0.74(7)	3059.7 → 2806.3	$(23/2^+) \rightarrow 21/2^+$
259.6	10	0.80(12)	2178.4 → 1918.8	$(13/2) \rightarrow (11/2)$
268.3	⩾10	0.75(8)	2880.6 → 2612.3	$(21/2^+) \rightarrow (19/2^+)$
269.0	⩾20		2612.3 → 2343.0	$(19/2^+) \rightarrow (17/2^+)$
269.3	56	0.56(6)	3329.2 → 3059.7	$(25/2^+) \rightarrow (23/2^+)$
270.5	⩽10	0.76(10)	2748.4 → 2477.9	$(19/2) \rightarrow (17/2)$
271.3	28	0.73(19)	3059.7 → 2788.4	$(23/2^+) \rightarrow 21/2^+$
274.2	38	0.72(7)	4641.7 → 4367.5	$(31/2^-) \rightarrow (29/2^-)$
274.5	17	0.80(11)	2590.1 → 2315.5	$(17/2) \rightarrow (15/2)$
274.6	166	0.75(7)	2343.0 → 2068.4	$(17/2^+) \rightarrow (15/2^+)$
275.5	⩾11	1.04(13)	3105.1 → 2829.7	$(21/2^+) \rightarrow (19/2^+)$
289.9	76	0.8(8)	2706.9 → 2417.0	$(19/2^+) \rightarrow (17/2^+)$
290.5	⩾20	0.78(7)	3171.2 → 2880.6	$(23/2^+) \rightarrow (21/2^+)$
293.8	32	1.36(13)	2650.5 → 2356.7	$(19/2^+) \rightarrow 19/2^+$
304.0	42	0.66(7)	3541.9 → 3237.9	$(25/2^+) \rightarrow (23/2^+)$
314.5	⩽10		5054.5 → 4740.0	$(33/2^+) \rightarrow (31/2^+)$
320.1	100	0.79(8)	3877.2 → 3557.1	$29/2^+ \rightarrow 27/2^+$
330.3	46	1.21(10)	2687.0 → 2356.7	$(19/2^+) \rightarrow 19/2^+$
343.0	55	0.82(8)	1893.7 → 1550.7	$15/2^- \rightarrow 13/2^+$
348.6	154	0.60(6)	2417.0 → 2068.4	$(17/2^+) \rightarrow (15/2^+)$
349.3	⩾10	0.75(18)	3056.2 → 2706.9	$(21/2) \rightarrow (19/2^+)$
354.8	79	1.50(10)	2423.2 → 2068.4	$(19/2^+) \rightarrow (15/2^+)$
357.3	⩾10	0.56(11)	3237.9 → 2880.6	$(23/2^+) \rightarrow (21/2^+)$
357.8	279	0.61(6)	2781.0 → 2423.2	$(21/2^+) \rightarrow (19/2^+)$
370.5	20	0.85(9)	3541.9 → 3171.2	$(25/2^+) \rightarrow (23/2^+)$
371.0	42	1.58(22)	2264.6 → 1893.7	$(15/2) \rightarrow 15/2^-$
378.9	17		4367.5 → 3988.6	$(29/2^-) \rightarrow (27/2^-)$
390.2	60	0.59(6)	3171.2 → 2781.0	$(23/2^+) \rightarrow (21/2^+)$
396.3	225	0.51(5)	1876.0 → 1479.7	$17/2^+ \rightarrow 15/2^+$
397.8	⩽10		4794.4 → 4396.6	$33/2^+ \rightarrow 31/2^+$
409.0	20	1.10(12)	3059.7 → 2650.5	$(23/2^+) \rightarrow (19/2^+)$
409.5	58	0.70(7)	4367.5 → 3958.0	$(29/2^-) \rightarrow (27/2^-)$
419.0			3207.2 → 2788.4	$(23/2^+) \rightarrow 21/2^+$
423.3	⩽10		4740.0 → 4316.7	$(31/2^+) \rightarrow (29/2^+)$

TABLE I. (*Continued.*)

E_γ(keV)[a]	I_γ[b]	R_{ADO}[c]	$E_i \rightarrow E_f$ (keV)[d]	$I_i^\pi \rightarrow I_f^\pi$[e]
428.0	22	0.85(8)	3329.2 → 2901.2	$(25/2^+) \rightarrow 23/2^+$
429.3	30	0.73(8)	3971.2 → 3541.9	$(27/2^+) \rightarrow (25/2^+)$
431.0	196	1.32(13)	2976.2 → 2545.2	$23/2^- \rightarrow 19/2^-$
431.5	35	0.57(6)	2788.4 → 2356.7	$21/2^+ \rightarrow 19/2^+$
437.2	38	0.81(9)	3283.5 → 2846.3	$(23/2^+) \rightarrow (21/2^+)$
441.1	170	0.70(7)	3557.1 → 3116.0	$27/2^+ \rightarrow 25/2^+$
449.6			2806.3 → 2356.7	$21/2^+ \rightarrow 19/2^+$
454.5	22	0.60(10)	3105.1 → 2650.5	$(21/2^+) \rightarrow (19/2^+)$
457.0	10		3237.9 → 2781.0	$(23/2^+) \rightarrow (21/2^+)$
466.8	$\leqslant$10	0.68(9)	3796.0 → 3329.2	$(27/2^+) \rightarrow (25/2^+)$
467.5	$\leqslant$10	0.74(11)	3215.9 → 2748.4	$(21/2) \rightarrow (19/2)$
472.5	$\geqslant$20		2829.7 → 2357.2	$(19/2^+) \rightarrow 17/2^+$
477.3	10		3283.5 → 2806.3	$(23/2^+) \rightarrow 21/2^+$
480.8	36	0.70(10)	2356.7 → 1876.0	$19/2^+ \rightarrow 17/2^+$
483.6	34	0.83(18)	3654.8 → 3171.2	$(25/2^+) \rightarrow (23/2^+)$
484.8	17	1.53(24)	3600.7 → 3116.0	$(25/2^+) \rightarrow 25/2^+$
490.4	1000	0.70(6)	1235.2 → 744.8	$11/2^- \rightarrow 9/2^+$
501.3	25		3672.5 → 3171.2	$\rightarrow (23/2^+)$
517.5	52	0.77(10)	2068.4 → 1550.7	$(15/2^+) \rightarrow 13/2^+$
518.5	$\leqslant$10		5160.2 → 4641.7	$\rightarrow (31/2^-)$
519.4	20	0.69(7)	4396.6 → 3877.2	$31/2^+ \rightarrow 29/2^+$
521.8	17	0.75(11)	2590.1 → 2068.4	$(17/2) \rightarrow (15/2^+)$
529.5	66	1.31(13)	2423.2 → 1893.7	$(19/2^+) \rightarrow 15/2^-$
544.5	252	1.27(13)	2901.2 → 2356.7	$23/2^+ \rightarrow 19/2^+$
547.2	225	0.76(7)	2423.2 → 1876.0	$(19/2^+) \rightarrow 17/2^+$
549.8	743	0.47(5)	1266.3 → 716.4	$13/2^+ \rightarrow 11/2^+$
561.8	40	0.51(5)	1306.5 → 744.8	$11/2^+ \rightarrow 9/2^+$
563.8	15		4120.9 → 3557.1	$\rightarrow 27/2^+$
593.3	1070	0.44(5)	651.0 → 57.4	$9/2^+ \rightarrow 7/2^+$
596.5	48		3377.5 → 2781.0	$\rightarrow (21/2^+)$
601.0	17	1.35(20)	5242.7 → 4641.7	$(35/2^-) \rightarrow (31/2^-)$
609.7	992	1.31(10)	1876.0 → 1266.3	$17/2^+ \rightarrow 13/2^+$
615.5	666	1.28(10)	1266.3 → 651.0	$13/2^+ \rightarrow 9/2^+$
628.5	$\geqslant$170	0.54(6)	628.5 → 0	$7/2^+ \rightarrow 5/2^+$
638.5	83	1.25(13)	2706.9 → 2068.4	$(19/2^+) \rightarrow (15/2^+)$
651.0	100	1.06(10)	651.0 → 0	$9/2^+ \rightarrow 5/2^+$
651.5	315	1.17(10)	2545.2 → 1893.7	$19/2^- \rightarrow 15/2^-$
653.1			4641.7 → 3988.6	$(31/2^-) \rightarrow (27/2^-)$
655.7	30	0.80(10)	1306.5 → 651.0	$11/2^+ \rightarrow 9/2^+$
656.0	$\leqslant$10		3557.1 → 2901.2	$27/2^+ \rightarrow 23/2^+$
658.5	637	1.22(10)	1893.7 → 1235.2	$15/2^- \rightarrow 11/2^-$
659.0	2647	1.23(10)	716.4 → 57.4	$11/2^+ \rightarrow 7/2^+$
667.3	72	1.44(14)	1973.8 → 1306.5	$15/2^+ \rightarrow 11/2^+$
678.0	161	1.33(13)	1306.5 → 628.5	$11/2^+ \rightarrow 7/2^+$
680.0	17		3796.0 → 3116.0	$(27/2^+) \rightarrow 25/2^+$
684.3	$\leqslant$10		1235.2 → 651.0	$11/2^- \rightarrow 9/2^+$
687.3	323		744.8 → 57.4	$9/2^+ \rightarrow 7/2^+$
688.8	99	0.55(11)	1924.0 → 1235.2	$(13/2) \rightarrow 11/2^-$
703.3	35	1.21(16)	3059.7 → 2356.7	$(23/2^+) \rightarrow 21/2^+$
707.5	22	0.70(8)	1973.8 → 1266.3	$15/2^+ \rightarrow 13/2^+$
738.0	$\leqslant$10	1.27(17)	5054.5 → 4316.7	$(33/2^+) \rightarrow (29/2^+)$
744.8	987	1.30(10)	744.8 → 0	$9/2^+ \rightarrow 5/2^+$
748.1	68	1.37(15)	3171.2 → 2423.2	$(23/2^+) \rightarrow (19/2^+)$
761.0	30	1.28(13)	3541.9 → 2781.0	$(25/2^+) \rightarrow (21/2^+)$
761.2	$\leqslant$10		3877.2 → 3166.0	$29/2^+ \rightarrow 25/2^+$
763.3	1230	1.20(10)	1479.7 → 716.4	$15/2^+ \rightarrow 11/2^+$
774.8	50	1.37(15)	4316.7 → 3541.9	$(29/2^+) \rightarrow (25/2^+)$
786.0	22		4343.1 → 3557.1	$\rightarrow 27/2^+$

TABLE I. (*Continued*.)

E_γ(keV)[a]	I_γ[b]	R_{ADO}[c]	$E_i \rightarrow E_f$ (keV)[d]	$I_i^\pi \rightarrow I_f^\pi$[e]
789.1	32	0.67(8)	2024.0 → 1235.2	$(13/2) \rightarrow 11/2^-$
802.1	460	0.72(7)	2068.4 → 1266.3	$(15/2^+) \rightarrow 13/2^+$
805.9	262	1.21(10)	1550.7 → 744.8	$13/2^+ \rightarrow 9/2^+$
806.4	65	1.21(15)	2357.2 → 1550.7	$17/2^+ \rightarrow 13/2^+$
812.3	30	1.42(15)	3600.7 → 2788.4	$(25/2^+) \rightarrow 21/2^+$
814.7	95	1.24(12)	3237.9 → 2423.2	$(23/2^+) \rightarrow (19/2^+)$
833.5	63	1.39(21)	2068.4 → 1235.2	$(15/2^+) \rightarrow 11/2^-$
834.2	72		1550.7 → 716.4	$13/2^+ \rightarrow 11/2^+$
839.5	38		4396.6 → 3557.1	$31/2^+ \rightarrow 27/2^+$
850.5	51	1.22(15)	3207.2 → 2356.7	$(23/2^+) \rightarrow 19/2^+$
855.8	$\geqslant$10		2829.7 → 1973.8	$(19/2^+) \rightarrow 15/2^+$
863.2	137	0.73(6)	2343.0 → 1479.7	$(17/2^+) \rightarrow 15/2^+$
877.0	581	1.22(10)	2356.7 → 1479.7	$19/2^+ \rightarrow 15/2^+$
894.8	26	1.50(36)	3796.0 → 2901.2	$(27/2^+) \rightarrow 23/2^+$
912.4	256	1.21(10)	2788.4 → 1876.0	$21/2^+ \rightarrow 17/2^+$
917.2	16	1.35(20)	4794.4 → 3877.2	$33/2^+ \rightarrow 29/2^+$
930.3	266	1.22(10)	2806.3 → 1876.0	$21/2^+ \rightarrow 17/2^+$
937.3	28	0.87(10)	2417.0 → 1479.7	$(17/2^+) \rightarrow 15/2^+$
939.5	$\leqslant$10		4316.7 → 3377.5	$(29/2^+) \rightarrow$
943.5	29	0.59(7)	2178.4 → 1235.2	$(13/2) \rightarrow 11/2^-$
956.3	24		3501.5 → 2545.2	$\rightarrow 19/2^-$
970.5	40	1.05(15)	2846.3 → 1876.0	$(21/2^+) \rightarrow 17/2^+$
981.8	88	1.23(10)	3958.0 → 2976.2	$(27/2^-) \rightarrow 23/2^-$
1012.5	45	1.20(12)	3988.6 → 2976.2	$(27/2^-) \rightarrow 23/2^-$
1029.5	29	1.24(17)	2264.6 → 1235.2	$(15/2) \rightarrow 11/2^-$
1085.5			3442.3 → 2357.2	$(21/2^+) \rightarrow 17/2^+$
1170.8	109	1.26(12)	2650.5 → 1479.7	$(19/2^+) \rightarrow 15/2^+$
1207.3	110	1.28(13)	2687.0 → 1479.7	$(19/2^+) \rightarrow 15/2^+$
1267.8	62	0.79(8)	1918.8 → 651.0	$(11/2) \rightarrow 9/2^+$
1307.5	100	0.86(8)	2024.0 → 716.4	$(13/2) \rightarrow 11/2^+$
1441.3	50	1.25(20)	2157.9 → 716.4	$(13/2) \rightarrow 11/2^+$
1461.8	21	0.74(11)	2178.4 → 716.4	$(13/2) \rightarrow 11/2^+$

[a]Uncertainties are between 0.1 and 0.5 keV.
[b]Uncertainties are within 30%.
[c]Extracted from $I_\gamma(37^\circ)/I_\gamma(90^\circ)$ in the coincidence spectra (see text for details).
[d]Excitation energies of initial E_i and final E_f states.
[e]Proposed spin and parity assignments for the initial I_i^π and final I_f^π levels.

interband transitions in band C and the 188.0-, 343.0-, and 834.2-keV linking transitions.

Band D consists of a strong $\Delta I = 1$ transition sequence along with several weak $\Delta I = 2$ crossover transitions. The 2901.2-keV level deexcites to two different $21/2^+$ states via 94.8- and 112.8-keV dipole transitions, and to the $19/2^+$ state via a 544.5-keV quadrupole transition leading to the $I^\pi = 23/2^\pm$ assignment for this level. The negative-parity assignment can be ruled out because it would require an $M2$ multipolarity for the 544.5-keV transition, which could not compete with the presumed 94.8- and 112.8-keV $E1$ transitions. Therefore, the $I^\pi = 23/2^+$ state is assigned for the 2901.2-keV level. The gated spectrum of Fig. 2(b) shows the transitions associated with band D. Additionally, several other levels identified in the present experiment are also included in Fig. 1 and labeled as structure E; this irregular level structure deexcites to bands B and D via γ rays of different energies and multipolarities.

Level structure F is built on the firmly established state at 2068.4 keV, which deexcites to bands A, C, and B via 174.7-, 517.5-, and 802.1-keV transitions respectively. The ADO ratio for the 174.7-keV transition is 1.20(12), in agreement with either a $\Delta I = 0$ or a $\Delta I = 2$ transition. However, the presence of the other two dipole (517.5- and 802.1-keV) linking transitions rejects an assignment of $\Delta I = 2$ for the 174.7-keV transition. Consequently, $I = 15/2$ for the 2068.4-keV level is preferred. Considering the possible quasiparticle configuration (see Sec. III D), we assigned positive parity for this level. A gated spectrum showing the existence of level structure F and its decay paths is shown in Fig. 2(d). The 290-, 357-, and 349-keV doublets are separated according to the coincidence relationships. The 269-keV line seems to be a triplet; two of the components are assigned in structure F, and the third one is placed in structure E feeding the $23/2^+$ state at 3059.7 keV. The placements and energies of these lines are confirmed by crossover transitions and energy sums as shown in Fig. 1.

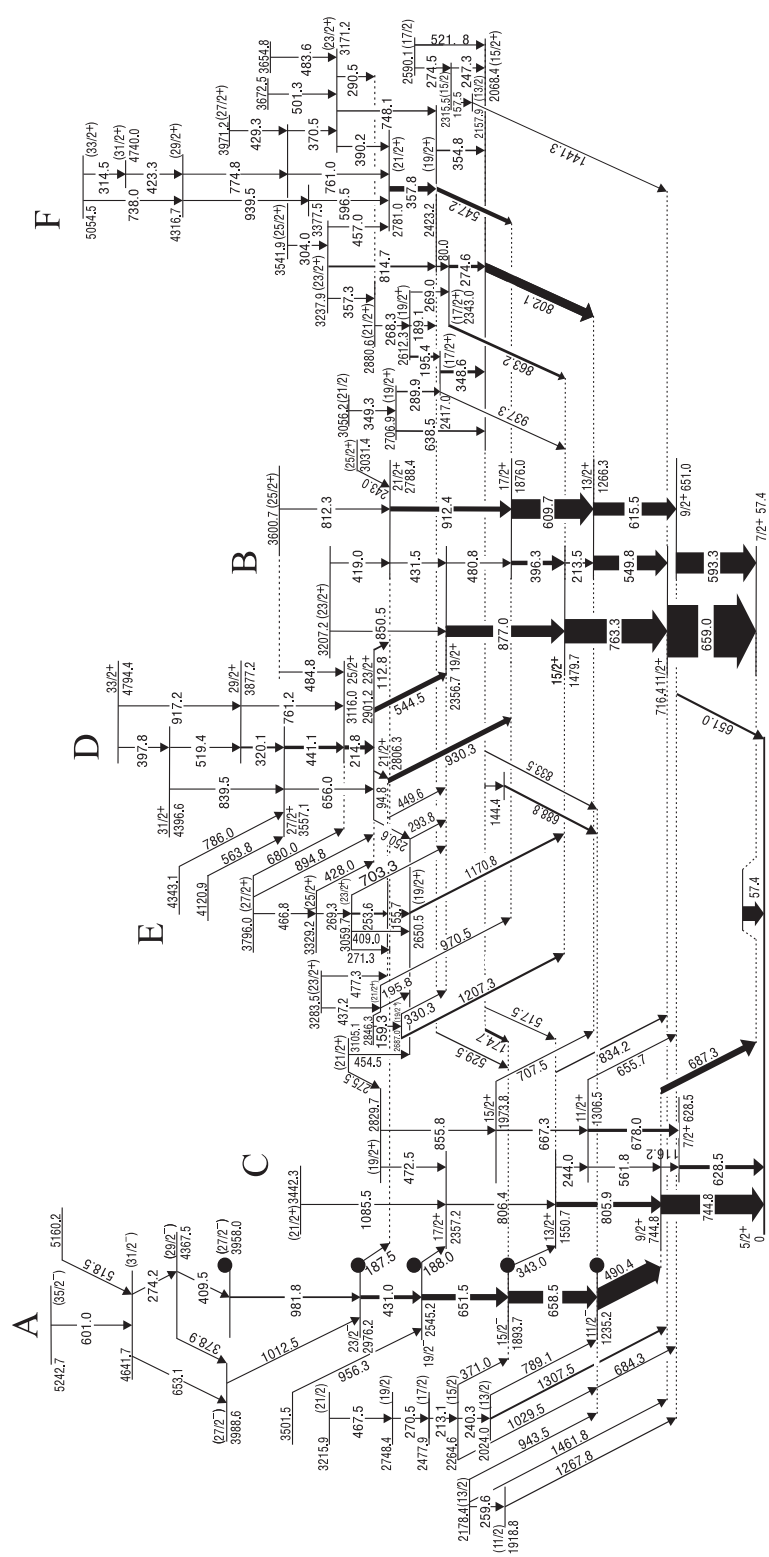

FIG. 1. Level scheme of ^{127}I deduced from this work. Excitation energies of $0^+, 2^+, \ldots, 8^+$ states in ^{126}Te [25] relative to $11/2^-$ level in ^{127}I are indicated as black dots.

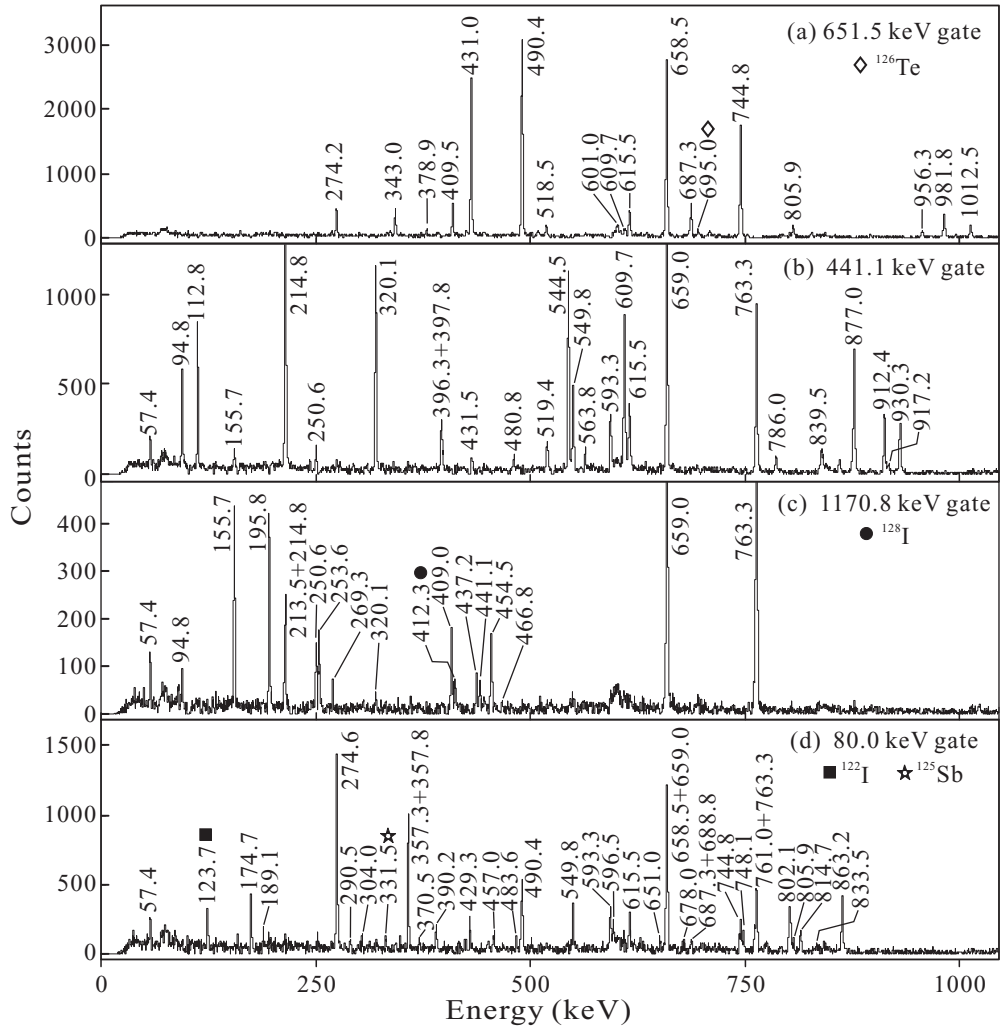

FIG. 2. Typical coincidence spectra with gates on selected transitions in band A and level structures D, E, and F as indicated on the panels. Note that there is a 651.0-keV transition depopulating band B, and the 609.7- and 615.5-keV transitions in band B appear in the spectrum gated by the 651.5-keV transition.

III. DISCUSSION

A. Preliminary remarks: slightly oblate deformation for the low-lying states

With three protons outside the $Z = 50$ shell closure, the transitional iodine isotopes are very soft against deformation and sensitive to the shape-polarizing effects of valence quasiparticles, and hence coexistence of different shapes can be expected in these nuclei. The shape coexistence phenomenon has generated considerable theoretical and experimental interest. In earlier theoretical studies, the Strutinsky-type calculations performed by Hagemann *et al*. revealed that the $\pi d_{5/2}(5/2^+)$, $\pi g_{7/2}(7/2^+)$, and $\pi h_{11/2}(11/2^-)$ intrinsic states in heavier odd-A iodine nuclei are slightly oblate, with deformation of $\beta_2 \sim -0.15$, whereas the $\pi g_{9/2}(9/2^+)$ configuration gives rise to a prolate deformed shape [19,20]. Later, the energies of the low-lying single-quasiparticle states were calculated for a range of iodine isotopes at both prolate and oblate deformations [6]. The calculations predicted competing oblate and prolate shapes for the $\pi d_{5/2}$, $\pi g_{7/2}$, and $\pi h_{11/2}$ configurations. The band heads built on these orbitals with oblate deformation decrease in energy as the neutron number N increases, and the oblate states become lower than the related prolate states when $N > 66$. Meanwhile, rotational bands based on the high-K oblate and low-K prolate $\pi h_{11/2}$ configuration were reported experimentally in ^{119,121}I [6] and oblate $\pi g_{7/2}/d_{5/2}$ bands were systematically observed in odd-A $^{121-125}$I [6–8]. The oblate deformation of those bands was determined from the experimental negative sign of the $E2/M1$ mixing ratios. In this mass region, for strongly coupled bands based on a single-quasiproton configuration, the sign of the $E2/M1$ mixing ratio δ for the interband $\Delta I = 1$ transitions is the same as the sign of the intrinsic quadrupole moment Q_0 [6]. Thus, negative δ values would indicate an oblate shape. Theoretically, band structures in heavier odd-A $^{121-127}$I can be well reproduced within the framework of the core-quasiparticle coupling model [2,9] and the particle-triaxial-rotor model, taking into account both prolate and oblate deformations [10,21]. These calculations also showed that the $\pi d_{5/2}$, $\pi g_{7/2}$, and high-Ω $\pi h_{11/2}$ configurations have an oblate deforma-

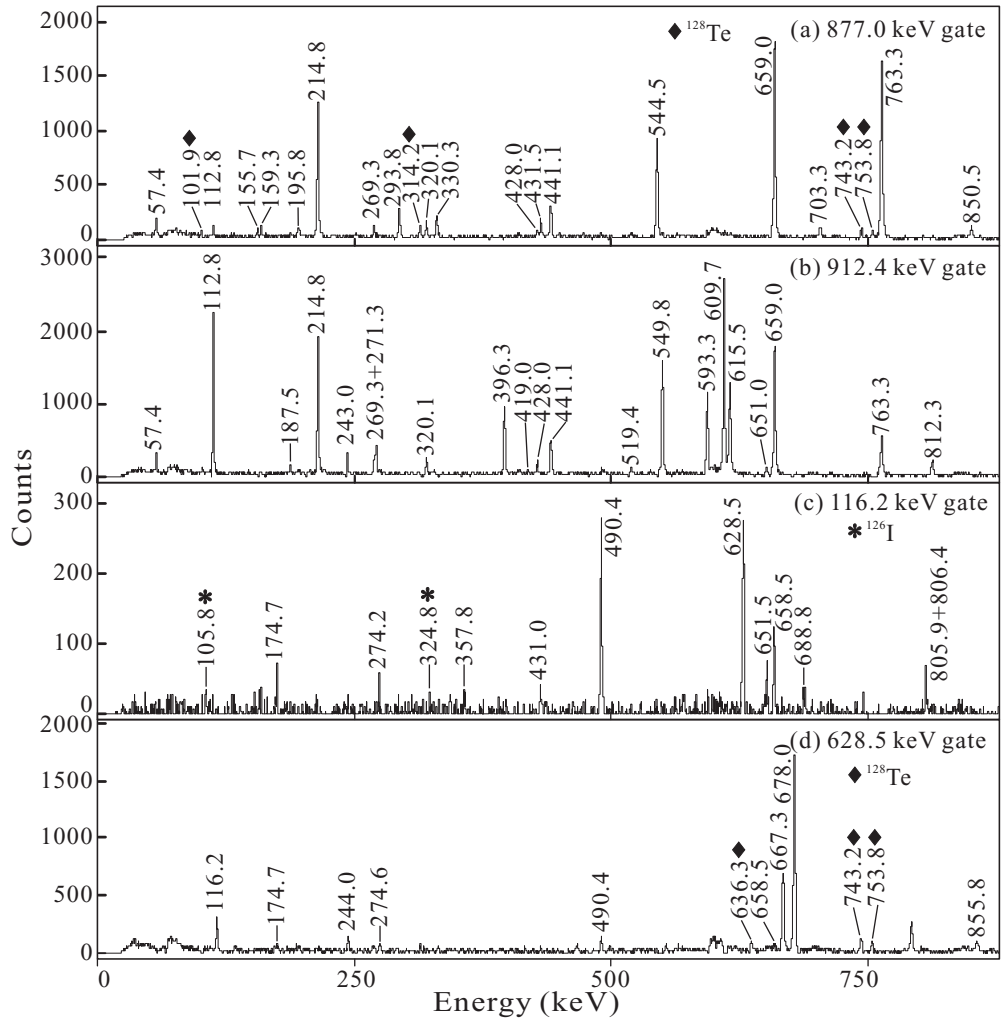

FIG. 3. Typical coincidence spectra with gates on selected transitions in bands B and C as indicated on the panels.

tion of $\beta_2 \sim -0.15$ [10,19–21]. In fact, the experimentally measured static quadrupole moments for the $I^\pi = 5/2^+$ and $7/2^+$ states in heavier odd-A $^{125-133}$I have negative sign [22]. Taking ^{127}I as an example, the measured static quadrupole moments for the $I^\pi = 5/2^+$ g.s. and the first excited $7/2^+$ state are -0.79 and -0.71 eb [22]. These results lead to the intrinsic quadrupole moments of -2.21 and -1.52 eb, respectively, assuming $K = I = 5/2$ and $K = I = 7/2$ for the two states. Considering the information mentioned above and the potential energy surface (PES) calculations (see Sec. III E for details), a slightly oblate shape of ^{127}I at low excitation energy is adopted in the following discussion.

B. One-quasiproton bands

1. *Decoupled band A based on the $\pi h_{11/2}$ configuration*

The negative-parity states labeled A in Fig. 1 are built on the $11/2^-$ state. An analogous sequence of $E2$ transitions built on the $11/2^-$ state has been observed in the odd-mass iodine isotopes with mass number A from 109 to 127 [5,23,24], and interpreted as decoupled bands originating from the proton $h_{11/2}$ orbital. These bands resemble the rotational characters of even-even xenon at low spins for the lighter iodine isotopes. Such negative-parity levels follow the same vibrational behaviors as the neighboring even-mass tellurium core states for the heavier isotopes with $A > 121$ [24]. In fact, the decoupled nature of these bands is inferred from the similar energy level spacings with those of the corresponding even-even cores. This is really the case comparing ^{127}I with ^{126}Te [25] in Fig. 1, where the level spacings in ^{126}Te are indicated by black dots. The striking similarity suggests that the negative-parity levels from $11/2^-$ through $27/2^-$ are formed by coupling the aligned $h_{11/2}$ proton to the core states from 0^+ through 8^+. The yrast 6^+ level in the tellurium core nuclei, which is unusually low in energy, is believed to be a two-QP noncollective state based on the $(\pi g_{7/2}/d_{5/2})^2$ configuration since the excitation energy of such a 6^+ level is nearly equal ($\sim$1.8 MeV) irrespective of mass number in the range $A = 120$–126 (see Fig. 4 in Ref. [26]). Accordingly, the $I^\pi = 23/2^-$ state in odd-A iodine was interpreted as being associated with the $\pi[h_{11/2}(g_{7/2}/d_{5/2})^2]$ configuration [27]. Similarly, the above-mentioned low-lying $23/2^-$ level in ^{127}I should be associated with the fully aligned $\pi[h_{11/2}(g_{7/2}/d_{5/2})^2]_{23/2^-}$ three-quasiproton configuration. For

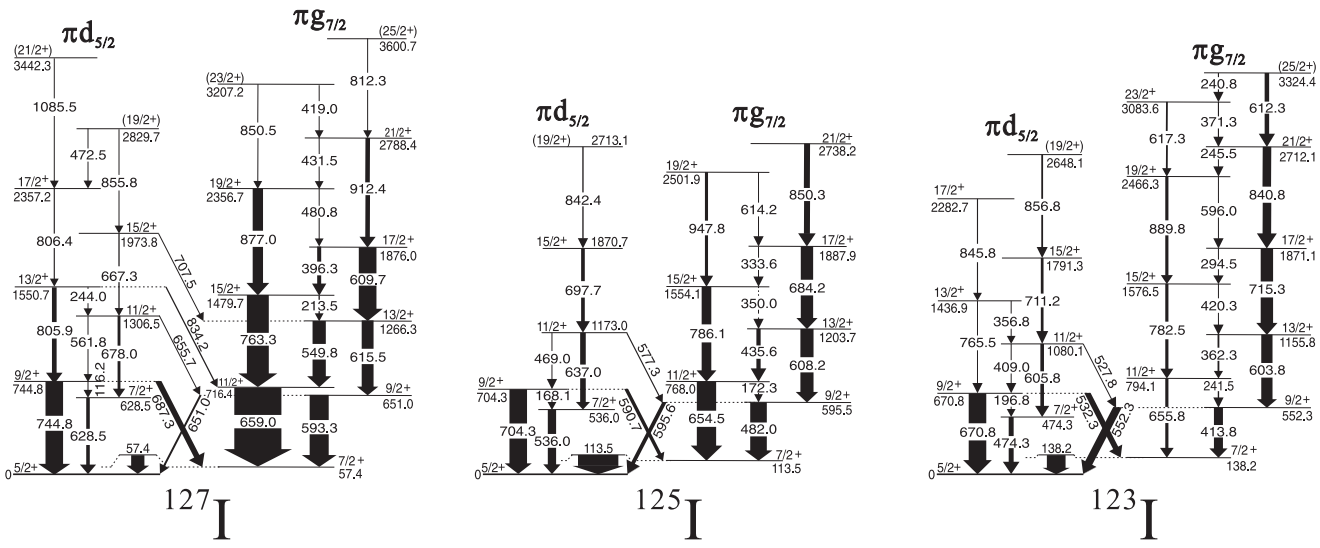

FIG. 4. Band structures based on the $\pi g_{7/2}$ and $\pi d_{5/2}$ orbitals in the odd-A ^{127,125,123}I isotopes (present work and Refs. [7,8]). The relative intensities are normalized to the $9/2^+_2 \rightarrow 5/2^+$ transition.

the higher spin states ($I \geqslant 27/2$), the irregular level spacings together with parallel and crossover transitions are observed. These observations indicate a structure change associated with quasineutron excitations involving most likely the $(\nu h_{11/2})^2$ contributions.

2. *Bands B and C associated with the $\pi g_{7/2}$ and $\pi d_{5/2}$ configurations*

The low-lying positive-parity states should be associated with the proton $d_{5/2}$ and $g_{7/2}$ configurations. The lowest $5/2^+$ and $7/2^+$ states were compared systematically in excited energies in odd-A $^{121-131}$I; the energy of the $7/2^+$ state relative to the $5/2^+$ state decreases monotonically with increasing neutron number, and the ordering of the two states becomes inverted in ^{127,129}I [19]. Such inversion indicates that the two states originate from the $\pi d_{5/2}$ and $\pi g_{7/2}$ single-proton orbitals respectively [7,19]. The two positive-parity $\Delta I = 2$ sequences of band B in ^{127}I built on the first $5/2^+$ (g.s.) and $7/2^+$ states were described previously as "decoupled bands," arising from the coupling of the odd proton in the $d_{5/2}$ and $g_{7/2}$ orbitals with the collective motion of the core [3,5]. However, the strong inter-band 593.3- and 549.8-keV transitions in the lower part of the bands suggest that these two $\Delta I = 2$ sequences have similar configurations, with a large overlap in their wave functions. In the present work, five new interband transitions are observed connecting states up to $23/2^+$ at 3207.2 keV. This observation strongly suggests that the two yrast $\Delta I = 2$ bands can be interpreted as signature partners of the same high-K configuration. The $\alpha = -1/2$ signature branch is favored in energy, therefore, the main component should be the $g_{7/2}$ proton configuration. Following this configuration assignment, the lowest $7/2^+$ state should be the band head of band B. As a consequence, the $5/2^+$ state should be the band head of another band, i.e., band C. Then, the 651.0-keV transition is assigned as a linking transition between bands B and C, as arranged in Fig. 1.

Based on the above analysis and the systematics of the similar bands in the neighboring ^{121,123,125}I isotopes [6–8], band B in ^{127}I is interpreted as being associated with the $7/2^+[404]$ oblate configuration originating from $\pi g_{7/2}$ subshell, with possible admixtures from the nearby $5/2^+[402]$ orbital arising from $\pi d_{5/2}$ subshell. Such a high-K orbital is responsible for the strong interband $\Delta I = 1$ transitions. The observed level staggering in this band may be caused by the mixing of the $\pi g_{7/2}$ and $\pi d_{5/2}$ configurations and the triaxial deformation as suggested in ^{123}I [28]. The oblate deformation for band B can be obtained experimentally from γ-ray angular distributions. The experimental $E2/M1$ mixing ratios reported for the 593.3-keV $9/2^+ \rightarrow 7/2^+$ and the 549.8-keV $13/2^+ \rightarrow 11/2^+$ transitions in band B have a negative sign (see Table III of Ref. [4]). One can see from Table I that the ADO values for the $\Delta I = 1$ transitions in band B are systematically smaller than that of pure dipole transitions ($\sim$0.75). This is also consistent with a negative $E2/M1$ mixing ratio for these transitions, implying a negative sign of quadrupole moment and an oblate deformation for band B.

The weakly populated positive-parity band labeled C is analogous to a $\Delta I = 1$ band known in ^{123}I which was interpreted as arising mainly from the $\pi d_{5/2}$ configuration at oblate deformation [7]. This interpretation for band C in ^{127}I could be adopted here. This band with the $\alpha = +1/2$ signature favored in energy shows properties similar to those discussed for band B, namely, the observation of interband $\Delta I = 1$ transitions and the consistently smaller ADO ratios for these $\Delta I = 1$ transitions (see Table I). Thus, the $5/2^+[402]$ high-K oblate configuration is assigned to band C.

The $\pi g_{7/2}$ and $\pi d_{5/2}$ bands are systematically observed in the odd-A $^{117-127}$I isotopes. As in cesium isotopes [12], the population strength of the two bands relative to the $\pi h_{11/2}$ band increases considerably with increasing neutron number. A reason could be that, with increasing neutron number, the

smaller deformation of nuclei will push the excitation energy of the $\pi h_{11/2}$ orbital up higher, thus making this band less yrast in the heavier isotopes. Figure 4 compares the level schemes of the $\pi d_{5/2}$ and $\pi g_{7/2}$ bands in $^{123-127}$I. For the $\pi d_{5/2}$ bands, the two signatures with several interband $\Delta I = 1$ transitions have been observed in ^{123,127}I, while only the $\alpha = -1/2$ signature branch was reported in ^{125}I (see Fig. 4). In view of the systematics shown in Fig. 4, it is reasonable to assign this band in ^{125}I to a similar oblate high-K $\pi d_{5/2}$ configuration, as in the neighboring ^{123,127}I nuclei rather than the prolate low-K configuration [29]. In fact, the oblate configuration assignment for this $\pi d_{5/2}$ band in ^{125}I was adopted in Ref. [30] as well. The experimentally observed $\pi g_{7/2}$ and $\pi d_{5/2}$ $\Delta I = 1$ bands in $^{121-127}$I could be predicted quite consistently within the core-quasiparticle coupling model [2,9] and the particle-triaxial-rotor model [10,21]. In this sense, it is necessary to search for the missing partner of the $\pi d_{5/2}$ band in ^{125}I for a further understanding of the band structure in ^{125}I.

C. Three-quasiparticle band D

A number of three-QP bands have been observed in odd-mass iodine and cesium nuclei in this mass region [6,8,11,12,31–36]. The band heads lie between 2.0- and 3.0-MeV excitation, with spins at $\sim 21/2$. In ^{127}I, the sequence of levels labeled D in Fig. 1 shows a bandlike structure built on the 2901.2-keV $23/2^+$ state; it consists of a strong dipole cascade along with weak $E2$ crossover transitions. This band is most probably associated with the breaking of an $h_{11/2}$ neutron pair, i.e., built on the $\pi g_{7/2} \otimes (\nu h_{11/2})^2$ configuration. This configuration assignment is based on the following considerations. First, the 4^+–10^+ levels in even-even tin [37] and the 8^+ and 10^+ states in even-even tellurium isotopes, such as in the neighboring ^{126,128}Te [25], were systematically observed, and a nearly pure $(\nu h_{11/2})^2$ configuration was proposed for these states. Second, the $23/2^+$ isomeric state at $E_x \sim 2.1$ MeV in ^{129,131}Sb was interpreted as the $\pi g_{7/2} \otimes (\nu h_{11/2})^2$ configuration [38]. Third, three-QP bands involving the $(\nu h_{11/2})^2$ configuration were commonly observed in this mass region for the odd-A iodine and cesium nuclei [11,30]. As an example, Fig. 5 presents a comparison between band D and the $\pi g_{7/2} \otimes (\nu h_{11/2})^2$ band in ^{125}I [30]. The similarity of transition energies can be clearly seen among the two bands. The close resemblance hence supports the same configuration assignment for band D as that in ^{125}I.

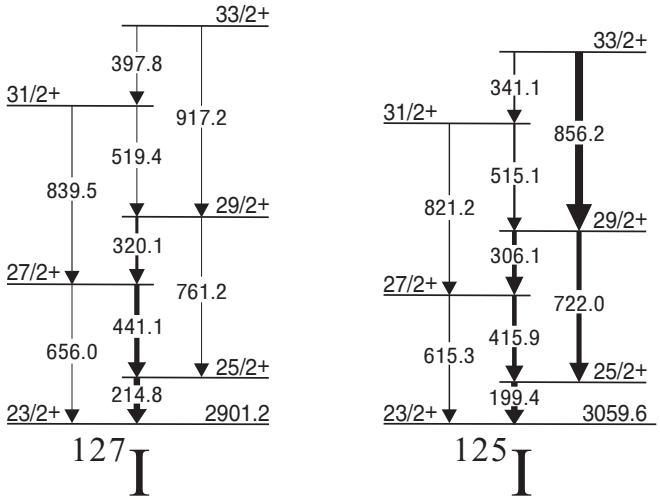

FIG. 5. Comparison of three-quasiparticle bands built on the $I^\pi = 23/2^+$ state in ^{127}I (present work) with that in ^{125}I (Ref. [30]). The relative intensities are normalized to the $25/2^+ \rightarrow 23/2^+$ transition.

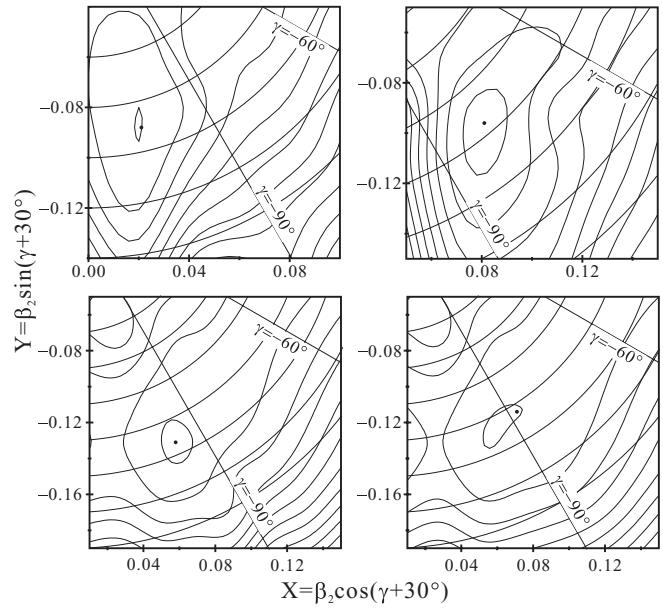

FIG. 6. PES calculations for the $I^\pi = 23/2^+$state (upper left), $I^\pi = 15/2^+$ state (upper right), lowest $I^\pi = 7/2^+$ state (lower left), and $I^\pi = 5/2^+$ ground state (lower right). Minima are indicated by black dots and the contour separation is 200 keV. The calculated deformations and excitation energies are given in Table II.

We notice the fact that three-QP bands of positive parity based on the $\pi h_{11/2} \otimes \nu(h_{11/2}g_{7/2})$ configuration were reported in $^{117-121}$I [6,31,32], and the band-head excitation energies increase from 2314 keV in ^{117}I to 3510 keV in ^{121}I due to increased $\pi h_{11/2}$ single-particle energies. In view of this systematic trend, the band head of such a three-QP band in ^{127}I would be located at ~ 5.5 MeV, which may be too high to be observed in this experiment. In fact, the excitation energy associated with the $\pi h_{11/2} \otimes \nu(h_{11/2}g_{7/2})$ configuration could reach up to ~ 6.6 MeV in our PES calculations (see Table II and Sec. III E for details). Therefore, it seems unlikely to assign the $\pi h_{11/2} \otimes \nu(h_{11/2}g_{7/2})$ configuration to band D. Apart from this, the $\pi g_{7/2} \otimes \nu(h_{11/2}g_{7/2})$ configuration, which was observed in ^{125}I [8] and ^{127}Cs [11], could not be associated with band D since this configuration should have a negative parity while a positive parity has been firmly determined for band D in this work.

D. Level structures E and F

The irregular level structure E, starting from relatively high spin ($I^\pi = 19/2^+$) and high excitation energy (2650.5 keV),

TABLE II. Calculated excitation energies E_{cal} (keV) and shapes of the lowest $5/2^+$, $7/2^+$, and possible three-quasiparticle states in ^{127}I. These are compared with the experimentally determined values, E_{exp}.

I^π	E_{exp}	E_{cal}	Configuration	β_2	$\lvert\gamma^\circ\rvert$	β_4
$5/2^+$	0	11	$\pi 5/2^+[402]$	0.134	88.121	0.02
$7/2^+$	57	0	$\pi 7/2^+[404]$	0.143	96.067	0.006
$15/2^+$	2068	3184	$\pi 3/2^+[411] \otimes \pi\{5/2^+[413] \otimes 7/2^+[404]\}_{6^+}$	0.121	76.184	−0.013
		2551	$\pi 3/2^+[422] \otimes \pi\{5/2^+[413] \otimes 7/2^+[404]\}_{6^+}$	0.075	82.231	−0.040
		1979	$\pi 3/2^+[422] \otimes \pi\{5/2^+[402] \otimes 7/2^+[404]\}_{6^+}$	0.126	79.669	−0.008
		1965	$\pi 3/2^+[411] \otimes \pi\{5/2^+[402] \otimes 7/2^+[404]\}_{6^+}$	0.136	83.582	−0.007
$23/2^+$	2901	6584	$\pi 7/2^-[523] \otimes \nu\{9/2^-[514] \otimes 7/2^+[404]\}_{8^-}$	0.071	102.344	−0.024
		4473	$\pi 5/2^+[413] \otimes \nu\{11/2^-[505] \otimes 7/2^+[404]\}_{9^-}$	0.070	102.196	−0.029
		2846	$\pi 3/2^+[422] \otimes \nu\{11/2^-[505] \otimes 9/2^-[514]\}_{10^+}$	0.090	106.719	−0.009
		2726	$\pi 3/2^+[411] \otimes \nu\{11/2^-[505] \otimes 9/2^-[514]\}_{10^+}$	0.074	104.137	0.027
		2690	$\pi 5/2^+[413] \otimes \nu\{11/2^-[505] \otimes 7/2^-[523]\}_{9^+}$	0.103	98.274	−0.007
		2166	$\pi 7/2^+[404] \otimes \nu\{11/2^-[505] \otimes 5/2^-[532]\}_{8^+}$	0.107	97.674	0.004
		1886	$\pi 7/2^+[404] \otimes \nu\{9/2^-[514] \otimes 7/2^-[523]\}_{8^+}$	0.112	98.001	0.003

is probably associated with three-QP excitations. These states are linked to bands B and D. A similar level structure in ^{125}I [30], also built on the $I^\pi = 19/2^+$ state at 2620 keV and feeding the yrast band, was observed and assigned to the $\pi g_{7/2} \otimes (\nu h_{11/2})^2$ configuration; two level structures of the same configuration in ^{125}I were suggested as arising from different triaxial deformations [30]. A similar interpretation could be adopted for the level structure E in ^{127}I, and our PES calculations for ^{127}I seem to support such an interpretation (see Sec. III E for details).

The level structure F built on the $15/2^+$ state displays irregular level spacings and many parallel decay branches. Among all these irregular levels, the 2068.4-keV $15/2^+$ level is most strongly populated. The $(\pi g_{7/2}/d_{5/2})^3$ three-QP configuration might be assigned to this $15/2^+$ level, given the fact that the two-QP states were observed in the neighboring even-even nuclei. Indeed, the yrast 6^+ states have been systematically observed in the even-even tellurium nuclei, such as in ^{126}Te, and a noncollective two-QP $(\pi g_{7/2}/d_{5/2})^2_{6^+}$ configuration has been assigned to these states [26]. As for ^{127}I, the $\pi g_{7/2}$ band is yrast; therefore, the positive-parity $(\pi g_{7/2}/d_{5/2})^3$ three-quasiproton configuration is favored for this $15/2^+$ level. This level decays mainly into the $13/2^+$ state in the $\pi g_{7/2}$ band via an intense $M1$ (802.1-keV) transition, which is consistent with the configuration assignment. This configuration assignment is further supported by the following PES calculations (see Sec. III E for details).

The maximum angular momentum formed by the $(\pi g_{7/2}/d_{5/2})^3$ three-QP configuration is $17/2^+$, and therefore the higher-spin states in level structure F should be associated with the coupling of three-QP configurations to the core excitations. Since it is much easier to align neutron pairs than to beak the $Z = 50$ closed shell, the higher noncollective states would involve the breaking of a neutron $h_{11/2}$ pair; i.e., the higher noncollective states in level structure F may be interpreted as five aligned valence nucleons outside a $^{122}_{50}$Sn$_{72}$ core, including three protons in the $\pi g_{7/2}/d_{5/2}$ orbitals and two neutrons in the $\nu h_{11/2}$ orbital. As mentioned in the previous section, the neutron two-QP $(\nu h_{11/2})^2 8^+$ states have been systematically observed in the even-even core nuclei; the excitation energy of such an 8^+ state in ^{126}Te (^{128}Te) is found to be 2766 (2689) keV. In the present experiment, the relative excitation energy of the 4740.0-keV $31/2^+$ state with respect to the 2068.4-keV $15/2^+$ state is 2671.4 keV which is almost the same as the excitation energy of the 8^+ state in the neighboring ^{126}Te (^{128}Te). This might indicate that the $31/2^+$ level at 4740.0 keV has the $(\pi g_{7/2}/d_{5/2})^3_{15/2^+} \otimes \nu(h_{11/2})^2_{8^+}$ configuration.

E. PES calculations

To have a deeper understanding of the three-QP configurations in ^{127}I as well as the collective (band D) and noncollective (level structures E and F) excitations, we have performed PES calculations using the configuration-constrained blocking method [39]. Single-particle levels are obtained from the nonaxial deformed Woods-Saxon potential with the set of universal parameters [40]. In the pairing treatment, particle-number projection is approximated by the Lipkin-Nogami method [41]. In order to obtain the configuration-dependent PES for a given multi-QP state, a process of adiabatic blocking is necessary, whereby the given orbitals that are occupied by the specified quasiparticles are followed and blocked. This has been achieved by calculating and identifying the average Nilsson quantum numbers for every orbital involved in a configuration [39]. For each quasiparticle configuration, the quadrupole and hexadecapole deformations, β_2, γ, and β_4, were varied in order to obtain the nuclear shape and to minimize the excitation energy. It has been shown that this method is very powerful for obtaining the right deformation and energy of a quasiparticle state [39,42].

Table II shows the results of PES calculations performed for the $I^\pi = 23/2^+$ and $I^\pi = 15/2^+$ three-QP states on which band structures D and F are built. For the $I^\pi = 23/2^+$ state, the calculated excitation energies for the $\pi h_{11/2} \otimes \nu(h_{11/2} g_{7/2})$ and $\pi g_{7/2} \otimes \nu(h_{11/2} g_{7/2})$ configurations are 6584 and 4473 keV, respectively. The former is much larger than the

latter since the $\pi g_{7/2}$ orbital is lower in energy than the $\pi h_{11/2}$ orbital. The two energies of 6584 and 4473 keV are both significantly higher than the experimental value of 2901 keV. On the other hand, the calculated energies associated with the $\pi g_{7/2} \otimes (\nu h_{11/2})^2_{8^+}$ configuration are lower than 2901 keV. As can be seen from Table II, the best agreement is found for the $I^\pi = 23/2^+$ state, assuming the $\pi 3/2^+[422] \otimes \nu\{11/2^-[505] \otimes 9/2^-[514]\}_{10^+}$ configuration. This is consistent with the $\pi g_{7/2} \otimes (\nu h_{11/2})^2$ configuration assignment for band D and indicates that the two $h_{11/2}$ neutrons are coupled to maximum 10^+ rather than 8^+. It should be noted that the $\pi 3/2^+[422]$ orbital could be mixed with the $\pi 3/2^+[411]$ orbital, as the calculated excitation energies of the two configurations are close to each other.

For the $I^\pi = 15/2^+$ state, the four possible combinations related to the $(\pi g_{7/2}/d_{5/2})^3$ three-quasiproton configuration have been calculated. The mixed $3/2^+[422]/3/2^+[411] \otimes 5/2^+[402] \otimes 7/2^+[404]$ three-quasiproton configuration is proposed for this state, as the predicted excitation energies for the two configurations are nearly equal (1979 and 1965 keV) and both are in good agreement with the experimentally observed value of 2068 keV.

As representative examples, the calculated PESs for the $I^\pi = 23/2^+$, $\pi 3/2^+[422] \otimes \nu\{11/2^-[505] \otimes 9/2^-[514]\}_{10^+}$ configuration and $I^\pi = 15/2^+$, $\pi\{3/2^+[422] \otimes 5/2^+[402] \otimes 7/2^+[404]\}$ configuration are shown in the upper part of Fig. 6, from which one can see that both surfaces are rather soft with respect to γ and β_2 deformations. In such a soft nucleus, competition between single-particle excitations and collective motions can be observed. In fact, coexistence of noncollective and collective level structures has been observed experimentally in the neighboring even-even $^{122-126}$Xe (see Ref. [43] and references therein) and in odd-A $^{115-119}$I isotopes [14,15,44]. Collective configurations are predicted to have deformations with $\gamma \sim 0^\circ$ or -50°. For noncollective states, theory predicts an oblate deformation with $\gamma \sim +60^\circ$ [43,45]. The observation of noncollective states was attributed to an oblate shell gap in the single-particle level diagram at $Z = 54$ [45]. From this point of view, the similar phenomenon observed in ^{127}I, i.e., collective (band D) and noncollective (level structures E and F) excitations coexist at similar energies, could be interpreted qualitatively.

It should be noted that the low- and medium-energy states in ^{127}I were studied theoretically in two very recent works, Refs. [46,47]. Toivanen *et al.* calculated the low-energy spectrum in ^{127}I by application of the nuclear shell model, and the $5/2^+$ g.s. and the lowest $7/2^+$ state were correctly predicted [47]. A more precise and more complete explanation for the previously observed states (up to an excitation energy of $\sim$3 MeV) was given by Zeghib [46] within the framework of a rotational (particle-rotor) model. The author pointed out that the so-called $\Delta I = 2$ bands of $\pi g_{7/2}$, $\pi d_{5/2}$, and $\pi h_{11/2}$ parentage could be naturally interpreted instead as being rotational multiplets assuming relatively small prolate deformation of $\delta = 0.12$ for the rotor. In the present work, the lowest $5/2^+$ and $7/2^+$ states were also calculated using the PES method, and it is instructive to compare the present results with the earlier ones. The calculated excitation energies shown in Table II agree satisfactorily with the experimental results, and are broadly consistent with the earlier calculations. Furthermore, the PESs show that the two states both have a small β_2 deformation of $\sim$0.13, in accordance with the value adopted in Ref. [46], whereas the calculated γ value ($\sim -90^\circ$) disagrees with the assumption of prolate deformation in Ref. [46]. In fact, the calculated PESs (shown in the lower part of Fig. 6) are found to be extremely γ soft with rather shallow minima, corresponding to the lowest $5/2^+$ and $7/2^+$ states, respectively.

Finally, it is worth mentioning that the strongly coupled $\Delta I = 1$ bands based on low-lying $\pi g^{-1}_{9/2} 9/2^+$ states have been systematically observed in iodine isotopes. The corresponding band in ^{127}I was reported by Shroy *et al.* in Ref. [4]. However, this band could not be confirmed in this work. In fact, no linking transitions between the $\pi g^{-1}_{9/2}$ band and the known states were observed in Ref. [4]. Moreover, such a $\Delta I = 1$ band has not been reported in the $N = 74$ isotones ^{129}Cs and ^{125}Sb [12,48]. This could be explained as follows: the expected smaller β_2 deformation in these nuclei will push up the energy of the $9/2^+[404]$ Nilsson orbital, hence making such a band occur far away from the yrast line and making it difficult to observe experimentally [49].

IV. SUMMARY

The high-spin states in ^{127}I have been reinvestigated via a conventional in-beam γ-spectroscopy experiment using the ^{124}Sn(^{7}Li, $4n\gamma$)^{127}I reaction. The previously reported level scheme has been revised and largely extended to high-spin states. Collective bands based on $h_{11/2}$, $g_{7/2}$, and $d_{5/2}$ single-quasiproton states have been identified. The level spacings of the negative-parity $\Delta I = 2$ sequence, built on $11/2^-$ state, are in good agreement with those of the yrast band in ^{126}Te core. This band is described as a decoupled band based on the $\pi h_{11/2}$ configuration, extending our knowledge of decoupled structures to the heaviest stable iodine isotope. For the positive-parity yrast levels, several strong $\Delta I = 1$ interband transitions connecting the two $\Delta I = 2$ sequences have been observed, indicating that these levels form a $\Delta I = 1$ band. This $\Delta I = 1$ band is proposed to be built predominantly on the slightly oblate $7/2^+[404]$ configuration originating from the $\pi g_{7/2}$ subshell. Another similar $\Delta I = 1$ band of positive parity has been identified and interpreted as being mainly from the $5/2^+[402]$ configuration arising from $\pi d_{5/2}$ subshell with slightly oblate deformation. In the higher-spin region, irregular noncollective and regular collective excitations built on the $I^\pi = 15/2^+$ and $23/2^+$ three-QP states, respectively, have been observed. The $(\pi g_{7/2}/d_{5/2})^3$ and $\pi g_{7/2} \otimes (\nu h_{11/2})^2$ configurations are assigned to the $15/2^+$ and $23/2^+$ states. The excitation energies of the two states can be well reproduced by the configuration-constrained PES calculations.

ACKNOWLEDGMENTS

The Authors wish to thank the staffs in the Institute of Physics and Tandem Accelerator Center, University of Tsukuba, Japan for their help and hospitality during the

experiment. This work was supported by the National Natural Science Foundation of China (Grants No. 10825522, No. 1073505010, and No. 10775158), the JSPS Invitation Program for Research in Japan (Grant No. L00515), the Major State Basic Research Development Program of China (Grant No. 2007CB815005), and the Chinese Academy of Sciences.

[1] E. S. Paul, C. W. Beausang, D. B. Fossan, R. Ma, W. F. Piel, Jr., N. Xu, L. Hildingsson, and G. A. Leander, Phys. Rev. Lett. **58**, 984 (1987).
[2] F. Dönau and U. Hagemann, Z. Phys. A **293**, 31 (1979).
[3] D. M. Gordon, M. Gai, A. K. Gaigalas, R. E. Shroy, and D. B. Fossan, Phys. Lett. B **67**, 161 (1977).
[4] R. E. Shroy, D. M. Gordon, M. Gai, D. B. Fossan, and A. K. Gaigalas, Phys. Rev. C **26**, 1089 (1982).
[5] M. Gai, D. M. Gordon, R. E. Shroy, D. B. Fossan, and A. K. Gaigalas, Phys. Rev. C **26**, 1101 (1982).
[6] Y. Liang, D. B. Fossan, J. R. Hughes, D. R. LaFosse, T. Lauritsen, R. Ma, E. S. Paul, P. Vaska, M. P. Waring, and N. Xu, Phys. Rev. C **45**, 1041 (1992).
[7] S-Y. Wang, T. Komatsubara, Y-J. Ma, K. Furuno, Y-H. Zhang, Y-Z. Liu, T. Hayakawa, J. Mukai, Y. Iwata, T. Morikawa, G. B. Hagemann, G. Sletten, J. Nyberg, D. Jerrestam, H. J. Jensen, J. Espino, J. Gascon, N. Gjørup, B. Cederwall, and P. O. Tjøm, J. Phys. G **32**, 283 (2006).
[8] H. Sharma, B. Sethi, R. Goswami, P. Banerjee, R. K. Bhandari, and J. Singh, Phys. Rev. C **59**, 2446 (1999); H. Sharma, B. Sethi, P. Banerjee, R. Goswami, R. K. Bhandari, and J Singh, *ibid.* **63**, 014313 (2000).
[9] L. G. Kostova, W. Andrejtscheff, L. K. Kostov, F. Dönau, L. Käubler, H. Prade, and H. Rotter, Nucl. Phys. A **485**, 31 (1988).
[10] R. Goswami, B. Sethi, M. S. Sarkar, and S. Sen, Z. Phys. A **352**, 391 (1995).
[11] Y. Liang, R. Ma, E. S. Paul, N. Xu, D. B. Fossan, and R. A. Wyss, Phys. Rev. C **42**, 890 (1990).
[12] S. Sihotra, K. Singh, S. S. Malik, J. Goswamy, R. Palit, Z. Naik, D. Mehta, N. Singh, R. Kumar, R. P. Singh, and S. Muralithar, Phys. Rev. C **79**, 044317 (2009).
[13] D. L. Balabanski, G. Rainovski, N. Blasi, G. Falconi, G. Lo Bianco, S. Signorelli, D. Bazzacco, G. de Angelis, D. R. Napoli, M. A. Cardona, A. J. Kreiner, and H. Somacal, Phys. Rev. C **56**, 1629 (1997).
[14] E. S. Paul, J. Simpson, H. Timmers, I. Ali, M. A. Bentley, A. M. Bruce, D. M. Cullen, P. Fallon, and F. Hanna, J. Phys. G **18**, 971 (1992).
[15] E. S. Paul, R. M. Clark, S. A. Forbes, D. B. Fossan, J. R. Hughes, D. R. LaFosse, Y. Liang, R. Ma, P. J. Nolan, P. H. Regan, P. Vaska, R. Wadsworth, and M. P. Waring, J. Phys. G **18**, 837 (1992).
[16] D. Ward, J. S. Geiger, and R. L. Graham, Phys. Lett. B **29**, 487 (1969).
[17] K. E. Apt, W. B. Walters, and G. E. Gordon, Nucl. Phys. A **152**, 344 (1970).
[18] K. Furuno, M. Oshima, T. Komatsubara, K. Furutaka, T. Hayakawa, M. Kedera, Y. Hatsukawa, M. Matsuda, S. Mitarai, T. Shizuma, T. Saitoh, N. Hashimoto, H. Kusakari, M. Sugawara, and T. Morikawa, Nucl. Instrum. Methods Phys. Res., Sect. A **421**, 211 (1999).
[19] U. Hagemann, H.-J. Keller, and H.-F. Brinckmann, Nucl. Phys. A **289**, 292 (1977).
[20] U. Hagemann, L. Käubler, H.-J. Keller, F. R. May, H. Prade, and F. Stary, Nucl. Phys. A **389**, 341 (1982).
[21] H. C. Song, Y. X. Liu, and Y. H. Zhang, Chin. Phys. Lett. **21**, 269 (2004).
[22] *Table of Isotopes*, 8th ed., edited by R. B. Firestone and V. S. Shirley (Wiley, New York, 1996).
[23] M. Petri, E. S. Paul, B. Cederwall, I. G. Darby, M. R. Dimmock, S. Eeckhaudt, E. Ganioğlu, T. Grahn, P. T. Greenlees, B. Hadinia, P. Jones, D. T. Joss, R. Julin, S. Juutinen, S. Ketelhut, A. Khaplanov, M. Leino, L. Nelson, M. Nyman, R. D. Page, P. Rahkila, M. Sandzelius, J. Sarén, C. Scholey, J. Sorri, J. Uusitalo, and R. Wadsworth, Phys. Rev. C **76**, 054301 (2007).
[24] C.-B. Moon, G. D. Dracoulis, R. A. Bark, A. P. Byrne, P. A. Davidson, A. N. Wilson, A. M. Baxter, T. Kibédi, and G. J. Lane, J. Korean Phys. Soc. **43**, S100 (2003).
[25] C. T. Zhang, P. Bhattacharyya, P. J. Daly, Z. W. Grabowski, R. H. Mayer, M. Sferrazza, R. Broda, B. Fornal, W. Króas, T. Pawlat, D. Bazzacco, S. Lunardi, C. Rossi Alvarez, and G. de Angelis, Nucl. Phys. A **628**, 386 (1998).
[26] C. S. Lee, J. A. Cizewski, D. Barker, G. Kumbartzki, R. Tanczyn, R. G. Henry, L. P. Farris, and H. Li, Nucl. Phys. A **530**, 58 (1991).
[27] C.-B. Moon, J. Korean Phys. Soc. **45**(4), 859 (2004).
[28] R. Goswami, B. Sethi, P. Banerjee, and R. K. Chattopadhyay, Phys. Rev. C **47**, 1013 (1993).
[29] H. Sharma and P. Banerjee, Phys. Rev. C **64**, 064310 (2001).
[30] P. Singh, S. Nag, A. K. Singh, H. Hübel, A. Al-Khatib, P. Bringel, C. Engelhardt, A. Neußer-Neffgen, I. Ragnarsson, M. P. Carpenter, R. V. F. Janssens, T. L. Khoo, T. Lauritsen, G. B. Hagemann, C. R. Hansen, B. Herskind, G. Sletten, A. Bracco, G. Benzoni, F. Camera, P. Fallon, R. M. Clark, P. Chowdhury, and H. Amro, Phys. Rev. C **82**, 034301 (2010).
[31] M. P. Waring, D. B. Fossan, J. R. Hughes, D. R. LaFosse, Y. Liang, R. Ma, P. Vaska, E. S. Paul, S. A. Forbes, R. Wadsworth, and R. M. Clark, Phys. Rev. C **48**, 2629 (1993).
[32] S. Törmänen, S. Juutinen, R. Julin, A. Lampinen, E. Mäkelä, M. Piiparinen, A. Savelius, A. Virtanen, G. B. Hegemann, Ch. Droste, W. Karczmarczyk, T. Morek, J. Srebrny, and K. Starosta, Nucl. Phys. A **613**, 282 (1997).
[33] A. K. Singh, H. Hubel, J. Domscheit, G. B. Hagemann, B. Herskind, D. R. Jensen, J. N. Wilson, R. Clark, M. Cromaz, P. Fallon, A. Gorgen, I. Y. Lee, A. O. Macchiavelli, D. Ward, H. Amro, W. C. Ma, J. Timar, and I. Ragnarsson, Phys. Rev. C **70**, 034315 (2004).
[34] S. Sihotra, R. Palit, Z. Naik, K. Singh, P. K. Joshi, A. Y. Deo, J. Goswamy, S. S. Malik, D. Mehta, C. R. Praharaj, H. C. Jain, and N. Singh, Phys. Rev. C **78**, 034313 (2008).
[35] K. Singh, Z. Naik, R. Kumar, J. Goswamy, D. Mehta, N. Singh, C. R. Praharaj, E. S. Paul, K. P. Singh, R. P. Singh, S. Muralithar, N. Madhavan, J. J. Das, S. Nath, A. Jhingan, P. Sugathan, and R. K. Bhowmik, Eur. Phys. J. A **25**, 345 (2005).
[36] K. Singh, S. Sihotra, S. S. Malik, J. Goswamy, D. Mehta, N. Singh, R. Kumar, R. P. Singh, S. Muralithar, E. S. Paul, J. A. Sheikh, and C. R. Praharaj, Eur. Phys. J. A **27**, 321 (2006).
[37] A. Insolia, N. Sandulescu, J. Blomqvist, and R. J. Liotta, Nucl. Phys. A **550**, 34 (1992).

[38] J. Genevey, J. A. Pinston, H. R. Faust, R. Orlandi, A. Scherillo, G. S. Simpson, I. S. Tsekhanovich, A. Covello, A. Gargano, and W. Urban, Phys. Rev. C **67**, 054312 (2003).
[39] F. R. Xu, P. M. Walker, J. A. Sheikh, and R. Wyss, Phys. Lett. B **435**, 257 (1998).
[40] W. Nazarewicz, J. Dudek, R. Bengtsson, T. Bengtsson, and I. Ragnarsson, Nucl. Phys. A **435**, 397 (1985).
[41] W. Satuła, R. Wyss, and P. Magierski, Nucl. Phys. A **578**, 45 (1994).
[42] F. R. Xu, P. M. Walker, and R. Wyss, Phys. Rev. C **59**, 731 (1999).
[43] A. Al-Khatib, H. Hübel, P. Bringel, C. Engelhardt, A. Neußer-Neffgen, G. B. Hagemann, C. R. Hansen, B. Herskind, G. Sletten, A. Bracco, F. Camera, G. Benzoni, P. Fallon, R. M. Clark, M. P. Carpenter, R. V. F. Janssens, T. L. Khoo, T. Lauritsen, P. Chowdhury, H. Amro, A. K. Singh, and R. Bengtsson, Eur. Phys. J. A **36**, 21 (2008).
[44] E. S. Paul, D. B. Fossan, K. Hauschild, I. M. Hibbert, P. J. Nolan, H. Schnare, J. M. Sears, I. Thorslund, R. Wadsworth, A. N. Wilson, J. N. Wilson, and I. Ragnarsson, Phys. Rev. C **59**, 1984 (1999).
[45] H. Timmers, J. Simpson, M. A. Riley, T. Bengtsson, M. A. Bentley, F. Hannat, S. M. Mullins, J. F. Sharpey-Schafer, and R. Wyss, J. Phys. G **20**, 287 (1994).
[46] S. Zeghib, Phys. Scr. **81**, 025201 (2010); **84**, 069501 (2011).
[47] P. Toivanen, M. Kortelainen, J. Suhonen, and J. Toivanen, Phys. Rev. C **79**, 044302 (2009).
[48] M.-G. Porquet, Ts. Venkova, R. Lucas, A. Astier, A. Bauchet, I. Deloncle, A. Prévost, F. Azaiez, G. Barreau, A. Bogachev, N. Buforn, A. Buta, D. Curien, T. P. Doan, L. Donadille, O. Dorvaux, G. Duchêne, J. Durell, Th. Ethvignot, B. P. J. Gall, D. Grimwood, M. Houry, F. Khalfallah, W. Korten, S. Lalkovski, Y. Le Coz, M. Meyer, A. Minkova, I. Piqueras, N. Redon, A. Roach, M. Rousseau, N. Schulz, A. G. Smith, O. Stézowski, Ch. Theisen, and B. J. Varley, Eur. Phys. J. A **24**, 39 (2005).
[49] L. Hildingsson, W. Klamra, Th. Lindblad, F. Lindblad, Y. Liang, R. Ma, E. S. Paul, N. Xu, D. B. Fossan, and J. Gascon, Z. Phys. A **340**, 29 (1991).